BULLETIN OF THE POLISH ACADEMY OF SCIENCES
TECHNICAL SCIENCES, Vol. 74(5), 2026, Article number: 2345
DOI: 10.24425/bpasts.2026.2345

Influence of compression ratio on the combustion and emission behavior of ultrasonically synthesized animal-fat biodiesel

Abdul Hakim JAVID[1]*, **S. Ashfaque AHMED**[2], **R. Nirmal KUMAR**[1], and **Syed Amjad AHMED**[1]

[1] Department of Mechanical Engineering, C. Abdul Hakeem College of Engineering and Technology, Melvisharam, Ranipet, Tamil Nadu 632509, India
[2] Department of Mechanical Engineering, Priyadarshini Engineering College, Vaniyambadi, Tamil Nadu 632751, India

Abstract. Animal-fat biodiesel is biodegradable, nontoxic, and offers advantages such as improved lubricity and higher cetane number when blended with diesel, while its typical drawbacks such as high viscosity and poor cold-flow behavior can be mitigated through blending and moderate engine optimization. In this study, a 20% animal-fat biodiesel blend (AFB20) was produced from slaughterhouse waste using base-catalyzed transesterification enhanced by a 20 kHz ultrasonic horn, which reduced reaction time from 3 hours (magnetic stirring) to 10 minutes. The ultrasonically synthesized AFB20 was tested in a single-cylinder, four-stroke, variable-compression-ratio diesel engine at compression ratios from 16.5:1 to 19.5:1. Operation at 19.5:1 was most favorable; brake specific fuel consumption improved by 6.7% relative to 16.5:1, and brake thermal efficiency increased to 35% due to enhanced atomization. Peak cylinder pressure reached 72.76 bar, and maximum heat release rate was 30.98 J/°CA, indicating shorter ignition delay. Unburnt hydrocarbons decreased by ~ 20%, and smoke opacity reduced significantly because of better oxidation, while NO_x increased moderately by about 9.5%. Overall, AFB20 operated at CR 19.5:1 demonstrated improved efficiency, lower fuel consumption, and cleaner combustion with only a moderate increase in NO_x emissions, highlighting its potential as a sustainable biodiesel blend for existing stationary and agricultural diesel engines without requiring hardware modification.

Keywords: combustion analysis; brake thermal efficiency; exhaust emission analysis; alternative fuel; ultrasonic transesterification.

1. INTRODUCTION

The rising demand and cost of diesel fuel have accelerated research into alternative fuels, with biodiesel widely examined as a sustainable CI-engine substitute. Minor adjustments to injection pressure, injection timing, and compression ratio (CR) are commonly employed to enhance combustion efficiency and reduce emissions.

A four-stroke single-cylinder CI engine evaluated at injection timings of 23°, 20°, 17°, and 14° bTDC showed reduced NO_x, CO, and HC along with higher brake thermal efficiency (BTE), CO_2, and smoke at 14° bTDC [1]. Studies on CR variation with B20 palm biodiesel indicate that increasing CR elevates in-cylinder pressure and BTE, with lower CO/HC/smoke but higher NO_x. Biodiesel generally exhibits lower smoke at reduced loads, whereas higher HC emissions arise from spray and viscosity effects.

Investigations on varying injection pressure (250–350 bar) with rapeseed and soybean methyl esters revealed reduced torque and power but lower smoke and CO, with NO_x rising at higher pressures. Tests on Karanja biodiesel blends in VCR engines showed that higher CR and fuel-injection pressure (FIP) increased BTE and reduced BSFC, with B20 closest to diesel performance [2]. Optimization of AFB20 identified 200 bar and 19° bTDC as favorable for improved performance and emissions [3]. Injection-timing variation (9°–18° bTDC) in a CRDI engine achieved peak efficiency at 15° bTDC with reduced NO_x and CO [4]. Multi-parameter optimization of CR, IP, and IT in a VCR engine improved BTE by 4.3% and reduced NO_x by 3.9% at full load, with 10% EGR optimal for AFB20 control [5]. Tests with watermelon biodiesel showed lower BTE and higher BSFC but reductions in UBHC, CO, and NO_x; higher CRs improved combustion due to viscosity and volatility effects [6]. Diesel-acetylene dual-fuel operation reported higher BTE and lower CO, HC, and smoke at 200 bar FIP [7].

Across diverse biodiesels, elevated CR consistently enhances combustion phasing, increases BTE, and reduces CO/HC/smoke, though NO_x typically rises at the highest CR. Combining CR increases with injection-parameter optimization, additives, or EGR can compensate for the lower calorific value of biodiesel and stabilize NO_x formation.

However, systematic evaluation of ultrasonically published bovine tallow AFB20 under four compression ratios (16.5:1, 17.5:1, 18.5:1, and 19.5:1) is not available in the published literature. Most previous VCR biodiesel studies used conventionally stirred biodiesel from poultry or mixed animal fats and reported limited CR optimization. The present work addresses this gap by: (i) producing ASTM-compliant bovine-tallow biodiesel using 20 kHz ultrasonic transesterification within 10 minutes; (ii) performing four-point CR optimization with detailed com-

*e-mail: ahjaveedindia@gmail.com

Manuscript submitted 2025-11-24, revised 2026-06-24, initially accepted for publication 2026-07-04, published in September 2026.

bustion, performance, and emission analysis without engine hardware modification. To the best of the authors' knowledge, this is the first study combining 20 kHz ultrasonic synthesis and systematic four-point CR optimization of bovine-tallow AFB20 in a Kirloskar VCR diesel engine.

2. EXPERIMENTAL METHODOLOGY

This study investigates the combustion, performance, and emission characteristics of a diesel engine operating on a 20% animal-fat biodiesel blend (AFB20). Bovine fat biodiesel (AFB100) was produced via base-catalyzed transesterification following ASTM D6751-22 and splash-blended with BS-VI diesel. Fuel properties, measured using ASTM/EN methods, satisfied IS 15607:2022 B20 specifications. Experiments were conducted on a single-cylinder, water-cooled VCR diesel engine at 1500 ± 10 rpm under varied compression ratios and loads. The compression ratio range of 16.5:1 to 19.5:1, with unit-step increments, was selected to include the standard factory compression ratio of 17.5:1 and to cover the operating range commonly used in VCR biodiesel studies on Kirloskar engines [A1, A2, A3]. The upper limit of 19.5:1 was chosen to obtain noticeable thermodynamic improvement while remaining within the safe operating design limits of the engine. Combustion, performance, and emission data were acquired using full instrumentation, with results averaged over three steady-state runs.

2.1. Preparation of the blend AFB20

Biodiesel was produced from bovine fat sourced from slaughterhouses in Vaniyambadi, Tamil Nadu, using base-catalyzed transesterification compliant with ASTM D6751-22. Raw tallow, initially semi-solid, was melted at 60–70°C and cooled to 45°C before reaction. Transesterification followed the standard alkali-catalyzed methanolysis of triglycerides

$$\text{Triglyceride} + 3\text{CH}_3\text{OH} \rightleftharpoons 3\,\text{FAME(biodiesel)} + \text{Glycerol} \quad \text{(catalyzedbyKOH)}.$$

An 8:1 methanol-to-oil molar ratio and 1 wt% KOH were used. Two methods were applied: (a) magnetic stirring at 50–55°C for 180 min, and (b) ultrasonic-horn transesterification (20 kHz, 750 W, 60% amplitude) at 55°C, achieving complete conversion in 10 min with significantly lower energy use. After reaction, the mixture was settled for 8 h to separate biodiesel and glycerol (Fig. 1). The ester layer was washed with warm distilled water and gravity-separated to obtain purified AFB100.

Fig. 1. Separation of reaction products into two distinct phases following transesterification and an 8-hour settling period

The fuel properties of the produced biodiesel were analyzed at Italab, Chennai, India, using standard ASTM and EN test methods. Details of the testing instruments and calibration standards used for each measurement are presented in Table 1. Comprehensive fuel property analysis (Table 1) confirmed that AFB100

Table 1
Fuel properties of AFB100 compared with ASTM D6751-22 limits

Property (ASTM/EN Method)	ASTM D6751 limit	Instrument/Calibration	Ultrasonic AFB100	Magnetic stirring AFB100
Flash point (D93)	≥ 93°C	PMCC tester; NIST-traceable PMCC reference fluid	138°C	136°C
Kinematic viscosity at 40°C (D445)	1.9–6.0 mm^2/s	Capillary viscometer; ASTM viscosity standards (S3/S6)	4.62	4.68
Acid number (D664)	≤ 0.50 mg KOH/g	Potentiometric titrator; KHP primary standard	0.37	0.39
Free glycerin (D6584)	≤ 0.020%	GC-FID; ASTM glycerin standard mix	0.01%	0.01%
Total glycerin (D6584)	‘0.240%	GC-FID; ASTM glycerin standard mix	0.18%	0.18%
Oxidation stability (EN 14112)	*geq*3 h	Rancimat; certified FAME reference	7.1 h	7.0 h
Cloud point (D2500)	Report	Cloud-point tester; certified reference fluid	16°C	16°C
Cold soak filterability (D7501)	≤ 360 s	CSFT apparatus; ASTM D7501 protocol	182 s	179 s
Water & sediment (D2709)	≤ 0.050 vol%	Centrifuge; calibrated volumetric tubes	0.02 vol%	0.02 vol%
Sulfur (D5453)	≤ 15 ppm	UV fluorescence analyzer; NIST sulfur standards	8 ppm	9 ppm
Cetane number (D6890)	≤ 47	IQT analyzer; n-hexadecane/HMN standards	62.4	61.9
Ca + Mg combined (EN 14538)	≤ 5 ppm	ICP-OES; multi-element standards	2.1 ppm	2.3 ppm
Phosphorus (D4951)	≤ 10 ppm	ICP-OES; phosphorus standard solution	< 1 ppm	< 1 ppm
Ester content (EN 14103)	*geq*96.5%	GC-FID; C17:0 standard FAME mix	96.90%	96.20%

produced via ultrasonic assistance satisfies all graded specifications of ASTM D6751-22 (including S15 sulfur grade and Group I metals) and exhibits properties identical to or marginally superior to those obtained by conventional stirring.

Because ultrasonic processing delivered identical fuel quality with an 18-fold faster reaction and 82% lower energy use, ultrasonic-derived AFB100 was selected for blending and all engine tests. AFB20 was prepared by splash-blending 20% (v/v) AFB100 with 80% BS-VI diesel and gently mixing for 10 min. The blend remained stable for 72 h and met all IS 15607:2022 B20 requirements.

The ultrasonic fuel achieved 96.9% ester content and satisfied ASTM D6751-22 requirements, whereas the magnetically stirred biodiesel achieved 96.2% and failed the specification. The higher ester conversion indicates lower residual glycerides and better combustion quality.

This study demonstrates, for the first time, the successful use of a 20 kHz ultrasonic horn to transesterify bovine slaughterhouse fat into ASTM-compliant B100 in just 10 min, offering a fast, energy-efficient, and scalable approach suitable for decentralized biodiesel production.

2.2. Fuel properties and preparation of biodiesel blends

The key physicochemical properties of neat petroleum diesel (PD100), pure animal fat biodiesel (AFB100), and the prepared blend are presented in Table 2.

Table 2
Physicochemical properties of diesel, animal fat biodiesel, and the AFB20 blend

Property	Unit	Diesel (PD100)	AFB100	AFB20 blend
Kinematic viscosity at 40°C	mm^2/s	2.8	5.0	3.71
Density at 15°C	kg/m^3	833	882	848
Flash point	°C	50	64	52
Fire point	°C	54	70	55
Cetane index	–	50	52	–
Calorific value	kJ/kg	42 500	39 400	41 600

Biodiesel blends were prepared for engine testing, with AFB20 obtained by mixing 80% (v/v) BS-VI diesel (≤ 10 ppm sulfur) with 20% (v/v) purified AFB100. The mixture was stirred at 500 rpm for 5 min to ensure complete miscibility. No phase separation occurred after 72 h at ambient conditions, confirming blend stability. The final blend, designated AFB20, met IS 15607:2022 B20 specifications and was used directly in all experiments, remaining fully compatible with BS-VI/Euro 6 diesel engines without hardware modification.

A 20% biodiesel blend (B20) was selected because it offers an optimal balance between renewable fuel utilization and engine performance. It provides sufficient oxygen for cleaner and more efficient combustion while maintaining stable engine operation. Unlike higher biodiesel blends, B20 avoids excessive viscosity and poor atomization, making it a widely accepted blend for balancing environmental benefits, fuel properties, and engine performance [8, 9].

2.3. Engine test rig

A single-cylinder, four-stroke, direct-injection, water-cooled diesel engine (Kirloskar, India) was employed for all performance, combustion, and emission trials. The engine is widely used in agricultural and genset applications in India and is representative of small stationary diesel power units. Detailed specifications are listed in Table 3.

Table 3
Technical specifications of the test engine

Parameter	Specification
Make & model	Kirloskar TV1, vertical, naturally aspirated
Number of cylinders	1
Stroke	Four-stroke
Bore × stroke	87.5 mm × 110 mm
Rated power	5.2 kW at 1500 r/min
Compression ratio (standard)	17.5:1
Fuel injection timing	21° bTDC (fixed)
Fuel injection pressure	200 bar
Cooling system	Water-cooled
Dynamometer	Eddy current, water-cooled (Bengaluru make)
Loading type	Electrical, 0–100% load in 25% steps

Although the engine is originally designed with a fixed compression ratio of 17.5:1, the test rig is equipped with a tilting-cylinder-block arrangement that permits variation of clearance volume (V_c) by adjusting piston top position, thereby enabling compression ratio (CR) changes from 12:1 to 20:1 without modifying the combustion chamber geometry. The compression ratio is calculated as

$$r_c = \frac{V_s + V_c}{V_c},$$

where V_s is the swept volume and V_c is the clearance volume. Engine load was applied and controlled using an eddy-current dynamometer coupled directly to the crankshaft. The test rig is fully instrumented with a piezoelectric pressure transducer (Kistler), crank-angle encoder (resolution 1° CA), thermocouple sensors (K-type), airflow meter, fuel flow sensor, and a high-speed data acquisition system (National Instruments). Exhaust emissions were measured using a five-gas automotive exhaust analyzer (AVL DiGas 444N).

A schematic diagram and photograph of the experimental setup are shown in Fig. 2. Figure 2a Schematic of the experimental engine test facility (adapted from [3]); (b) Photograph of the actual test rig with eddy-current dynamometer and instrumentation. All tests were conducted at a constant engine speed of 1500 ± 10 r/min under steady-state conditions. Fuel

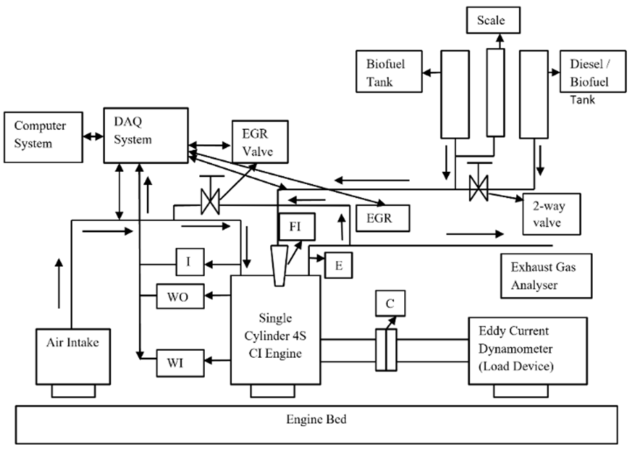

(a) FI-Fuel Injector, I-Intake Valve, E-Exhaust Valve, C-Coupling, WO-Water Outlet, WI-Water Inlet

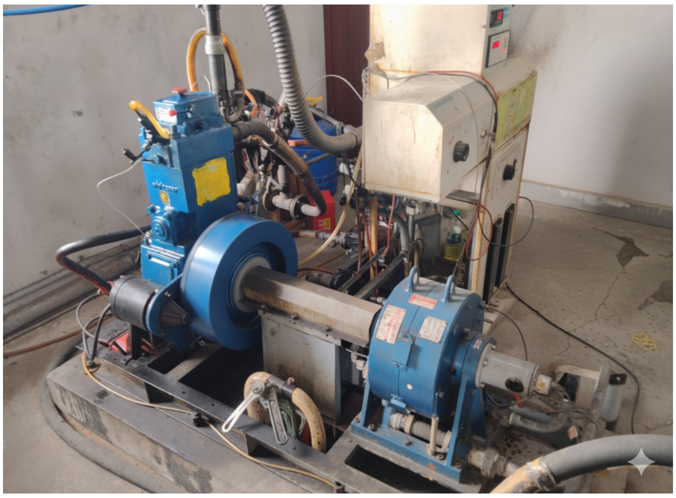

(b)

Fig. 2. (a) Schematic of experimental setup [3], (b) VCR engine test rig

injection timing (21° bTDC) and injection pressure (200 bar) were held constant at their standard settings across all four compression ratios, so that CR was the sole independent variable in this study. Each data point reported represents the average of three repeated measurements taken after attaining thermal stability (cooling water temperature 80 ± 2°C, lubricating oil temperature 90 ± 2°C).

Short-duration steady-state testing was performed in this study, whereas long-term durability and injector deposit formation at peak pressure and temperature were not conducted during this study.

2.4. Uncertainty analysis

Experimental uncertainty arises from instrument calibration tolerances, measurement imprecision, and inter-run variability. Uncertainty analysis was performed for all performance (BTE, BSFC), emission (CO, NO_x, UBHC, smoke), and combustion (cylinder pressure, HRR) parameters across all four tested compression ratios. Each test condition was repeated three times under thermally stabilized operation (cooling water 80 ± 2°C; lubricating oil 90 ± 2°C), and results were averaged.

The true value of a measured quantity x is expressed as

$$x' = x \pm U_x (P\%),$$

where x' is the true value, x the measured value, U_x the measurement uncertainty, and $P\%$ the confidence level. The combined uncertainty is obtained from bias error B_x (manufacturer calibration tolerance) and precision error P_x (repeatability)

$$U_x = \sqrt{\left(B_x^2 + P_x^2\right)}.$$

For derived parameters dependent on two or more independent measured quantities (e.g., BTE from brake power, fuel mass flow rate, and calorific value), uncertainty was propagated using

$$U_{y/y} = \sqrt{\left[\left(\frac{ux_1}{x_1}\right)^2 + \left(\frac{ux_2}{x_2}\right)^2 + \ldots + \left(\frac{ux_n}{x_n}\right)^2\right]}.$$

The overall uncertainty of the experimental system was evaluated as

$$U_{\text{overall}} = \pm\sqrt{\begin{Bmatrix} U_{\text{N}}^2 + U_{\text{CO}}^2 + U_{\text{NO}_x}^2 + U_{\text{UBHC}}^2 + U_{\text{Smoke}}^2 \\ + U_{\text{EGT}}^2 + U_{\text{BTE}}^2 + U_{\text{BSFC}}^2 + U_{\text{HRR}}^2 + U_{P_c}^2 + U_{\theta}^2 \end{Bmatrix}},$$

where N is engine speed, CO, NO_x, UBHC, and smoke are emission gases, and EGT is emission gas temperature. Instrument specifications, measurement techniques, and calibration accuracies are listed in Table 4.

Table 4
Description of instruments, measurement techniques, and calibration accuracy

Parameter	Instrument	Accuracy (Measurement range)
Load	Load cell – strain gauge	±0.1 kg (0–20 kg)
Engine speed	Speed sensor – magnetic pickup	±10 rpm (0–10 000 rpm)
Temperature	Temperature indicator – K-type thermocouple	±1°C (0–1200°C)
CO	AVL DiGas 444N – NDIR technique	0.01% vol (0–10% vol)
CO_2	AVL DiGas 444N – NDIR technique	0.1% vol (0–20% vol)
UBHC	AVL DiGas 444N – FID technique	1 ppm / 10 ppm (0–20 000 ppm)
NO_x	AVL DiGas 444N – CLD technique	±1% FS (0–5000 ppm)
Smoke	AVL 437 smoke meter – NDIR technique	±0.10% (0–100 %)
Cylinder pressure	Kistler piezoelectric pressure transducer	±0.1 bar (0–250 bar)
Crank angle	Optical incremental encoder	±1° CA (0–720° CA)

Computed uncertainty values for all parameters at each compression ratio are presented in Table 5. Uncertainty varies slightly across CRs because elevated compression alters in-cylinder pressure, temperature, and combustion stability, which in turn affects instrument signal quality and inter-run scatter. All measured parameters are within the permissible uncertainty limit of ±5% across all tested compression ratios.

Table 5
Uncertainty values and accuracy levels for all engine parameters range across compression ratios 16.5:1 to 19.5:1 (AFB20)

Parameter (accuracy ±)	Uncertainty (%) (CR 16.5:1 to 19.5:1)
CO emission (±0.01% vol)	0.10–0.14
NO_x emission (±10 ppm)	0.15–0.28
UBHC emission (±10 ppm)	0.20–0.38
Exhaust gas temp. (±1°C)	0.18–0.24
Smoke meter – HSU (±0.1%)	0.44–0.72
Brake thermal efficiency (–)	0.26–0.36
BSFC (±0.5 g/kWh)	0.30–0.48
Heat release rate (–)	0.36–0.52
Pressure transducer (±0.1 bar)	0.10 (all CRs)
Load cell (±50 g)	0.12–0.18
Engine speed (±10 rpm)	0.15–0.18
Measuring burette (±0.25 cc)	0.35–0.44
Crank angle encoder (±1° CA)	0.03–0.04
Overall uncertainty	1.48–1.78%

3. RESULTS AND DISCUSSION

3.1. Brake specific fuel consumption (BSFC)

Figure 3 presents the variation of brake specific fuel consumption (BSFC) with brake power for the AFB20 blend at four different compression ratios (CR 16.5:1, 17.5:1, 18.5:1, and 19.5:1). Compared with neat diesel (PD100), AFB20 showed higher BSFC across all loads due to its lower heating value. However, increasing the compression ratio reduced this difference, indicating improved combustion efficiency. For all tested compression ratios, BSFC decreased progressively with increasing load, which is typical of diesel engine behavior due to the relatively constant frictional losses and improved volumetric efficiency at higher loads.

At full load, the highest compression ratio (CR 19.5:1) produced the lowest BSFC in the present study (0.258 kg·kW^{-1}·h), representing a 6.7% reduction versus CR 16.5:1 (0.276 kg·kW^{-1}·h) and a 2.3% reduction versus the standard CR 17.5:1 (0.264 kg·kW^{-1}·h). The direction and magnitude of this change are consistent with prior experimental work showing that modest increases in CR (≈ 17 → 18–19) reduce specific fuel consumption by improving combustion phasing, raising peak temperature/pressure, and shortening ignition delay [10, 11]. Quantitatively, a ≈ 6.25% improvement in SFC for

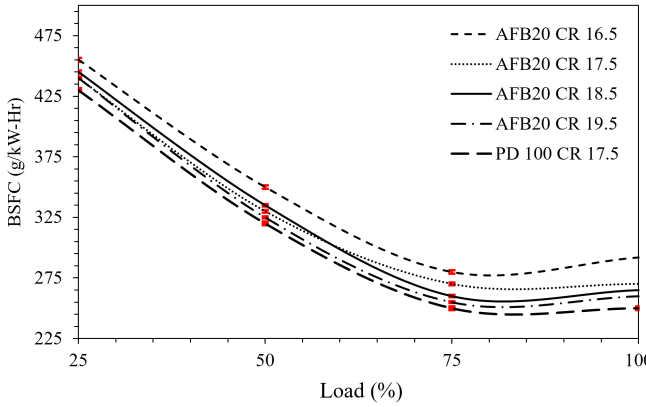

Fig. 3. Values of brake specific fuel consumption against load at various compression ratios. Error bars represent ±expanded uncertainty (Table 5)

a B20 sea-mango biodiesel blend at CR 18:1 versus CR 17:1 was reported [12], while another study with WCB20 exhibited a ≈ 5.9% BSFC advantage over petroleum diesel at selected speeds and noted clear compression-ratio–dependent behavior in BSFC. These verified observations indicate that the present-study reduction of 6.7% at CR 19.5:1 aligns with reported experimental values for biodiesel B20 blends when CR is increased by ∼ 1–2 units.

3.2. Brake thermal efficiency (BTE)

Figure 4 shows the variation of BTE with brake power for AFB20 at compression ratios (CR) of 16.5:1–19.5:1. Compared with neat diesel (PD100), AFB20 exhibited slightly lower BTE at all loads. However, increasing the compression ratio improved the thermal efficiency of AFB20, and at the highest compression ratio its BTE approached that of diesel, indicating more effective conversion of fuel energy into useful work. BTE increased with load for all CRs, consistent with diesel engine behavior where frictional losses become less significant, and combustion efficiency improves at higher loads (Heywood, 2018). Similar load-dependent trends for animal-fat biodiesels were reported [13].

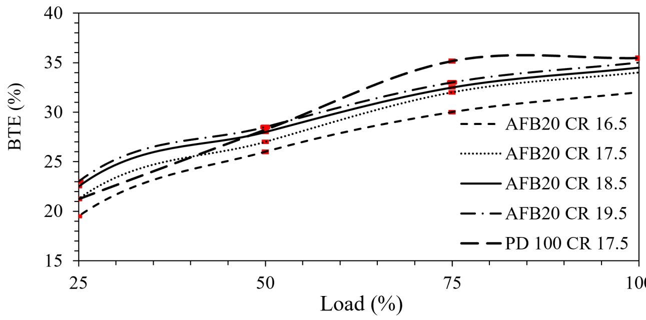

Fig. 4. Values of brake thermal efficiency against load at various compression ratios. Error bars represent ± expanded uncertainty (Table 5)

The highest BTE of 35% occurred at CR 19.5:1, exceeding CR 17.5:1 and 16.5:1 by 0.89% and 0.95%, respectively, while the lowest full-load BTE (∼ 32%) appeared at CR 16.5:1. Literature shows comparable improvements: increasing CR from $\sim 16:1$ to 19:1 yields 2.1–3.4% higher BTE for animal-fat B20 blends [14], with peak efficiencies of 34–35% at CR $\approx 19:1$ also reported for tallow and poultry-fat biodiesels (Srinivasan *et al.*, 2022).

At higher compression ratios, the increase in in-cylinder pressure and temperature leads to greater heat transfer to the cylinder walls, piston crown, and cylinder head, along with a slight rise in piston ring and bearing friction losses. However, within the investigated compression ratio range (16.5:1–19.5:1), the benefits obtained from improved combustion are greater than these additional losses. Higher CR improves combustion phasing and enables faster and more complete combustion closer to TDC, thereby reducing incomplete combustion losses and improving the overall energy conversion efficiency.

This behavior is reflected in the increase in BTE from approximately 32% to 35% and the lower exhaust gas temperature observed at CR 19.5:1, which indicates that a larger portion of the fuel energy is converted into useful work rather than being lost through the exhaust. Hence, although heat transfer and friction losses increase slightly at higher CR, the overall indicated-to-brake efficiency conversion remains favorable for AFB20 within the studied operating range.

3.3. Cylinder pressure (CP)

Figure 5 shows the full-load in-cylinder pressure (CP) traces of AFB20 for compression ratios (CR) from 16.5:1 to 19.5:1. Compared with neat diesel (PD100), AFB20 exhibited slightly lower peak cylinder pressure at the standard compression ratio. However, increasing the compression ratio progressively increased the peak pressure of AFB20, and at the highest compression ratio it exceeded that of diesel, indicating enhanced combustion intensity and improved energy release near TDC. Peak CP rises steadily with CR, increasing from 67.74 bar at CR 16.5:1 to 72.76 bar at CR 19.5:1 (~ 7.4% increase). This trend results from higher end-of-compression temperature and pressure, which intensify premixed combustion and shift more heat release near TDC. Similar CR-driven increases in CP and heat-release rates for biodiesel blends were reported by [10].

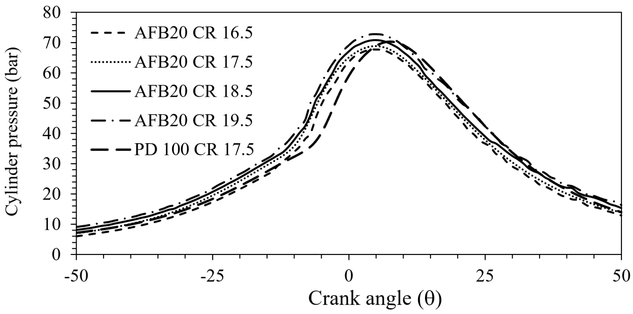

Fig. 5. Cylinder pressure with crank angle at various compression ratios. Measurement uncertainty for cylinder pressure was ±0.1% (Table 5)

The behavior aligns with biodiesel combustion characteristics: oxygenated fuels such as animal-fat methyl esters promote stronger premixed burn and steeper pressure-rise profiles [15] and exhibit shorter ignition delay due to higher saturation levels [11]. VCR-engine studies also confirm that B20 blends show higher CP at elevated CR because of improved air–fuel mixing and faster ignition phasing [12,16]. The progressive CP increase from CR 16.5:1 to 19.5:1 is consistent with established biodiesel combustion mechanisms and supports CR optimization for enhanced combustion efficiency with animal-fat biodiesel.

3.3.1. Implications for mechanical loads at elevated CR

The higher peak cylinder pressure observed at elevated compression ratios increases the mechanical loading on engine components such as the piston, connecting rod, and bearings. At CR 19.5:1, the 7.4% rise in peak pressure improves combustion performance but may also increase cyclic stresses and thermal loading during prolonged operation. However, animal-fat biodiesel blends generally provide better lubricity than diesel, which can help reduce component wear [17]. Previous VCR engine studies have also shown that such pressure increases remain within the normal structural limits of conventional diesel engines under stable combustion conditions [18]. Therefore, AFB20 operation at CR 19.5:1 appears mechanically feasible, though long-term durability evaluation is recommended.

3.4. Heat release rate (HRR)

Figure 6 shows that the heat release rate (HRR) of AFB20 increases markedly with compression ratio (CR). Compared with neat diesel (PD100), AFB20 exhibited a lower peak heat release rate at the standard compression ratio. However, increasing the compression ratio progressively increased the HRR and advanced its occurrence, and at the highest compression ratio the peak HRR approached that of diesel, indicating enhanced premixed combustion and improved combustion phasing. Peak HRR rises from 25.65 J/°CA at CR 16.5:1 to 30.98 J/°CA at CR 19.5:1 – a 20.8% increase – and the HRR peak shifts earlier, indicating stronger and better-phased premixed combustion. Higher CR elevates end-of-compression temperature and pressure, shortening ignition delay and causing more accumulated fuel to burn rapidly, producing a sharper premixed HRR peak [19].

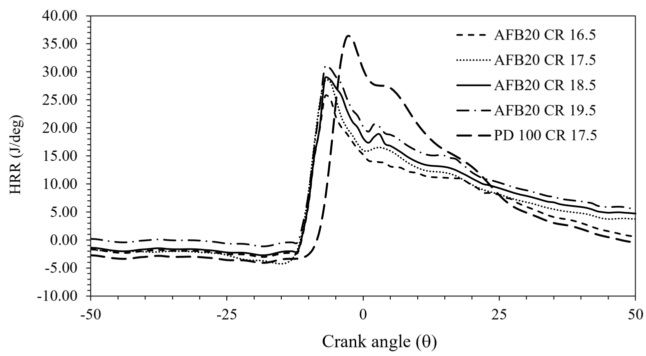

Fig. 6. Heat release rate versus crank angle at various compression ratios. Measurement uncertainty for HRR was within ±0.36−0.52% (Table 5)

AFB20 saturated FAME content and high cetane number further intensify this effect, supporting faster low-temperature oxidation [15]. Mid-range CRs (17.5:1 and 18.5:1) show similar HRR values, a plateau commonly observed in biodiesel VCR studies [11, 12]. Only at CR 19.5:1 does HRR rise sharply again as premixed-fuel accumulation reaches a threshold.

The observed HRR increase aligns with previous findings for waste-oil and sea-mango biodiesels, where higher CR consistently enhances premixed burn intensity [10, 12, 20]. Overall, elevating CR to 19.5:1 significantly strengthens premixed combustion and improves the thermodynamic efficiency potential of saturated animal-fat biodiesel blends.

3.5. Exhaust gas temperature (EGT)

Compared with neat diesel (PD100), AFB20 exhibited higher EGT across all loads, owing to its different combustion characteristics and lower heating value. However, increasing the compression ratio progressively reduced the EGT of AFB20, indicating more effective heat utilization and improved combustion efficiency. Figure 7 shows that exhaust gas temperature (EGT) increases with load for all compression ratios (CR) but decreases slightly as CR increases. The highest EGT occurs at CR 16.5:1, while CR 19.5:1 shows the lowest values, giving an average reduction of about 0.85% across loads. Higher CR lowers EGT because improved end-of-compression temperature and pressure shorten ignition delay, increase premixed combustion, and shift more heat into useful work rather than exhaust losses [19].

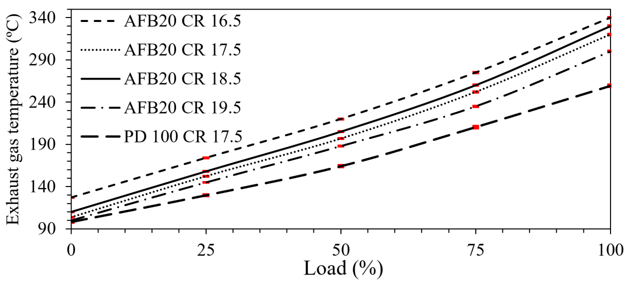

Fig. 7. Exhaust gas temperature vs load at various compression ratios. Error bars represent ± expanded uncertainty (Table 5)

This behavior is consistent with biodiesel VCR studies, which report that higher CR improves combustion phasing and thermal efficiency, thereby reducing exhaust energy even as peak pressure and HRR rise [10, 12]. Reactivity and oxygen content of biodiesel also influence EGT trends, with higher-cetane, oxygenated fuels showing greater heat-to-work conversion and lower exhaust temperatures at elevated CR [11]. This small but consistent EGT decrease at CR 19.5:1 agrees with verified findings that compression-ratio optimization reduces exhaust losses and enhances combustion efficiency in biodiesel-fueled CI engines [10].

3.6. Carbon monoxide (CO) emission

Compared with neat diesel (PD100), AFB20 produced higher CO emissions at full load. However, increasing the compression ratio reduced CO emissions, indicating more complete combustion. Figure 8 shows that CO emissions for AFB20 remain low and largely independent of compression ratio (CR) up to 75% load but rise sharply at full load. The highest CO (0.18% vol.) occurs at CR 16.5:1, while the lowest (0.12% vol.) is at CR 18.5:1, a 33% reduction. The full-load CO increase results from fuel-rich pockets and limited oxygen availability, compounded by the higher viscosity and poorer spray atomization of animal-fat methyl esters [15].

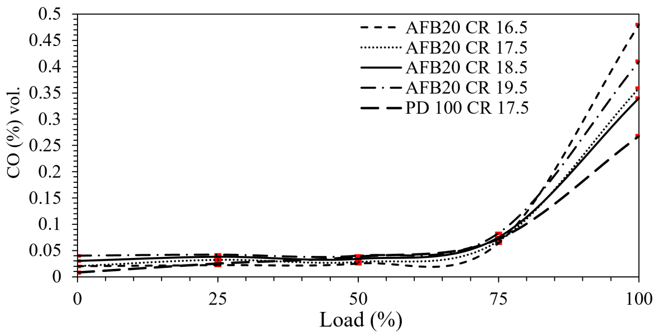

Fig. 8. CO emission versus load for the AFB20 blend at different compression ratios. Error bars represent ±expanded uncertainty (Table 5)

Raising CR reduces CO because higher in-cylinder temperatures and pressures improve $CO \rightarrow CO_2$ oxidation, shorten ignition delay, and enhance mixture preparation [19]. This behavior matches results from VCR studies showing lower CO at higher CR for biodiesel blends due to improved combustion phasing and reduced unburned carbon [10, 11]. Recent B20 investigations also report CO minimization near CR $\approx 18.5:1$ without excessive mechanical loading [12, 21]. Moderate CR elevation, especially to $\sim 18.5:1$, significantly improves CO oxidation for AFB20 at full load, consistent with established biodiesel combustion literature.

3.7. Unburned hydrocarbon (UBHC) emissions

Compared with neat diesel (PD100), AFB20 produced lower UBHC emissions across the load range. Furthermore, increasing the compression ratio reduced UBHC emissions, indicating more complete oxidation of unburned fuel. Figure 9 shows the variation of unburned hydrocarbon (UBHC) emissions with brake power for the AFB20 blend at different compression ratios. UBHC increased with load for all CRs due to higher fuel delivery and locally richer mixtures at elevated power. A clear decreasing trend in UBHC with rising compression ratio was observed in the present data: the highest UBHC occurred at CR 16.5:1 while the lowest occurred at CR 19.5:1, with CR 19.5:1 exhibiting 13.5% lower UBHC than CR 16.5:1 at full load and CR 17.5:1 and CR 18.5:1 showing intermediate reductions of 9.6% and 9.8%, respectively. The reduction in UBHC at higher compression ratios is attributable to elevated in-cylinder temperatures and pressures that enhance post-flame oxidation of hydrocarbons trapped in crevices, quench layers and oil films, while reduced clearance volume and stronger turbulence improve air–fuel mixing and oxidation completeness [19]. The oxygenated character and relatively high cetane tendency of many animal-fat methyl esters further promote earlier ignition

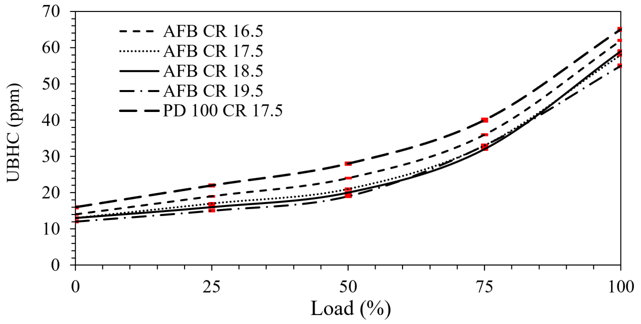

Fig. 9. Variation of unburnt hydrocarbon with load for the AFB20 blend at different compression ratios. Error bars represent ±expanded uncertainty (Table 5)

and more complete oxidation, which helps suppress UBHC under high-CR conditions.

The reduction in UBHC emissions at higher compression ratios is mainly due to improved post-flame oxidation of hydrocarbons trapped in crevice regions, reduced wall-quench effects, and oxygen-assisted combustion from the FAME component of AFB20. At CR 19.5:1, the higher in-cylinder temperature promotes more complete oxidation of crevice-trapped hydrocarbons and reduces quench-layer thickness near the cylinder wall [22]. In addition, the oxygenated nature of AFB20 enhances oxidation of partially burned fuel. As a result, UBHC emissions decreased by 13.5% at CR 19.5:1 compared to CR 16.5:1, consistent with established HC formation mechanisms in CI engines [19].

3.8. Oxides of nitrogen (NO_x) emission

The variation of NO_x emissions with brake power for the AFB20 blend across different compression ratios is presented in Fig. 10. Compared with neat diesel (PD100), AFB20 exhibited lower NO_x emissions across the entire load range. However, increasing the compression ratio slightly increased NO_x emissions, owing to the higher in-cylinder temperatures associated with improved combustion. NO_x increases with both engine load and compression ratio, with the highest NO_x at CR 19.5:1 and the lowest at CR 16.5:1, and CR 19.5:1 showing 9.5% higher NO_x than CR 16.5:1 at full load. NO_x formation in compression-ignition engines is governed primarily by thermal (Zeldovich) routes that are exponentially sensitive to peak combustion temperature, oxygen availability, and high-temperature residence time; higher CR elevates end-of-compression temperatures and pressures, shortens ignition delay and advances combustion phasing, all of which tend to raise NO_x production [19]. CR 19.5:1 in the present study yields performance and combustion benefits; the observed ∼ 9.5% NO_x increase relative to CR 16.5:1 is consistent with verified literature and suggests that practical implementation should consider mitigation strategies such as moderate EGR and injection timing retardation to balance thermal efficiency gains against NO_x formation [11, 19].

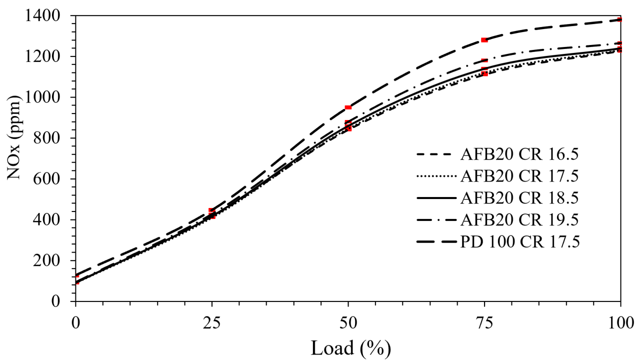

Fig. 10. Variation of NO_x emissions with brake power for the AFB20 blend at different compression ratios. Error bars represent ±expanded uncertainty (Table 5)

3.9. NO_x mitigation strategies for AFB20 at high CR

Although CR 19.5:1 produced the best overall combustion and performance characteristics for AFB20, it also resulted in approximately 9.5% higher NO_x emissions compared to CR 16.5:1. This increase can be effectively controlled using suitable NO_x reduction techniques reported in earlier studies on animal-fat biodiesel blends [23–26]. One of the commonly adopted methods is exhaust gas recirculation (EGR), where a small portion of exhaust gases is recirculated back into the intake air. The use of moderate EGR rates (about 5–10%) helps reduce peak combustion temperature and oxygen concentration inside the cylinder, thereby suppressing thermal NO_x formation without significantly affecting engine efficiency [23, 24]. Another effective approach is slight retardation of injection timing to around 18–19° bTDC, which delays the combustion process and lowers the duration of high-temperature heat release responsible for NO_x formation [25]. In addition, the use of antioxidant additives has been found to reduce combustion intensity and improve fuel oxidation stability, leading to further reduction in NO_x emissions [26]. Therefore, the higher NO_x emissions associated with CR 19.5:1 can be minimized through these practical mitigation strategies while still retaining the advantages of improved thermal efficiency and cleaner combustion obtained with the AFB20 blend.

3.10. Mechanistic attribution: Thermal vs. prompt NO_x for AFB20 at high CR

NO_x formation in CI engines mainly occurs through thermal and prompt mechanisms, with thermal NO_x being the dominant pathway during diesel combustion. At CR 19.5:1, the higher in-cylinder temperature and advanced combustion phasing increase the peak combustion temperature and the duration of high-temperature gases, resulting in the observed 9.5% increase in NO_x emissions [19].

The contribution of prompt NO_x is comparatively smaller in the case of AFB20. The higher compression ratio shortens ignition delay and reduces the premixed combustion phase where prompt NO_x is mainly formed. Moreover, bovine-tallow biodiesel contains predominantly saturated FAME compounds with low polyunsaturation, which limits CH-radical formation associated with the Fenimore mechanism [27]. Hence, the NO_x increase observed at higher CR is mainly thermal in nature.

3.11. Smoke

Compared with neat diesel (PD100), AFB20 exhibited higher smoke opacity across the load range. However, increasing the compression ratio reduced smoke emissions, indicating improved fuel oxidation and reduced soot formation. The variation of smoke opacity with brake power for the AFB20 blend at different compression ratios is shown in Fig. 11. Smoke emissions increased steadily with load for all CRs because of higher fuel delivery and the formation of richer local mixtures at elevated power output. However, a decreasing trend was observed with increasing compression ratio, with smoke levels progressively reducing from CR 16.5:1 to CR 19.5:1 across the full load range. At full load, CR 19.5:1 produced 22.5% lower smoke opacity than CR 16.5:1 and 5.1% lower opacity than CR 17.5:1, demonstrating a strong inverse relationship between smoke formation and compression ratio.

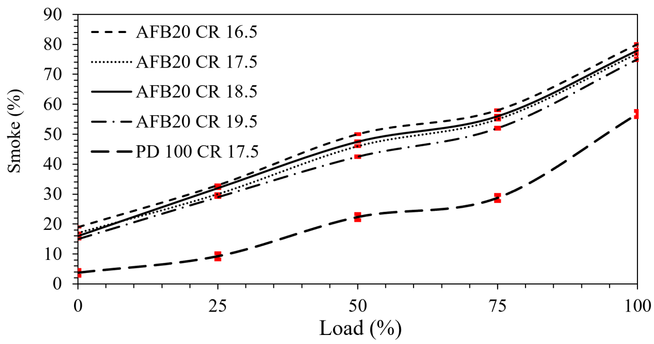

Fig. 11. Smoke opacity versus brake power for the AFB20 blend at different compression ratios. Error bars represent ±expanded uncertainty (Table 5)

The reduced smoke at higher CR is primarily governed by increased in-cylinder temperature and pressure, which improves atomization, promotes faster fuel vaporization, and enhances premixed-phase combustion, thereby reducing soot precursor formation and accelerating soot oxidation during diffusion combustion [19]. The inherent oxygen content of biodiesel further supports oxidation of nascent soot particles, particularly under the elevated thermodynamic conditions produced at higher compression ratios [10].

Results demonstrate that CR 19.5:1 is highly effective in reducing smoke emissions from saturated animal-fat B20 blends by leveraging improved thermodynamic conditions and the oxygenated chemistry of biodiesel.

4. CONCLUSIONS

Experiments conducted on a single-cylinder VCR diesel engine fueled with ultrasonically produced AFB20 showed that compression ratio strongly influences the combustion, performance, and emission characteristics of saturated biodiesel blends. Among the tested conditions, CR 19.5:1 delivered the best overall results, including a 6.7% reduction in BSFC, peak BTE of 35.0%, maximum cylinder pressure of 72.76 bar, and the highest heat release rate due to shorter ignition delay and improved premixed combustion. Exhaust gas temperature was also lowest at this CR, indicating improved thermal efficiency. CO, UBHC, and smoke emissions decreased significantly at higher CR, with UBHC and smoke opacity reducing by nearly 20% and 22.5%, respectively, compared to CR 16.5:1. Although NO_x emissions increased moderately (≈ 9.5%) at CR 19.5:1, the blend still demonstrated a favorable balance between efficiency improvement and emission reduction.

The study also demonstrates the effectiveness of 20 kHz ultrasonic transesterification for producing ASTM-compliant bovine-tallow biodiesel within only 10 minutes, offering a faster and more energy-efficient alternative to conventional stirring methods. In addition, the present work provides a systematic four-point compression-ratio optimization of ultrasonically derived AFB20 with detailed combustion, performance, and emission analysis. Overall, the results establish CR 19.5:1 as the optimal operating condition for bovine-tallow AFB20 in a Kirloskar VCR diesel engine without requiring engine hardware modification, highlighting the practical potential of ultrasonically derived animal-fat biodiesel as a sustainable drop-in fuel for existing stationary and agricultural diesel-engine applications.

REFERENCES

[1] M. Mani and G. Nagarajan, "Influence of injection timing on performance, emission and combustion characteristics of a DI diesel engine running on waste plastic oil," *Energy*, vol. 34, no. 10, pp. 1617–1623, Oct. 2009, doi: 10.1016/j.energy.2009.07.010.

[2] H.K. Amarnath, P. Prabhakaran, S.A. Bhat, and R. Paatil, "A Comparative Analysis of Thermal Performance And Emission Characteristics of Methyl Esters of Karanja And Jatropha Oils Based on A Variable Compression Ratio Diesel Engine," *Int. J. Green Energy*, vol. 11, no. 7, pp. 675–694, Aug. 2014, doi: 10.1080/15435075.2013.777905.

[3] S.A. Ahmed, I. Rahamathullah, and M.I. Ahmed, "Investigations on animal fat biodiesel selected blend by varying the fuel injection pressures and timings in the four-stroke single cylinder compression ignition engine," *Int. J. Ambient Energy*, vol. 45, no. 1, Dec. 2024, doi: 10.1080/01430750.2024.2414117.

[4] V.T. Lamani, A.K. Yadav, and K.N. Gottekere, "Performance, emission, and combustion characteristics of twin-cylinder common rail diesel engine fuelled with butanol-diesel blends," *Environ. Sci. Pollut. Res.*, vol. 24, no. 29, pp. 23351–23362, Oct. 2017, doi: 10.1007/s11356-017-9956-7.

[5] M. Krishnamoorthi and R. Malayalamurthi, "Combined Effect of Compression Ratio, Injection Pressure, and Injection Timing on Performance and Emission of a DI Compression Ignition Engine Fueled with Diesel–Aegle Marmelos Oil–Diethyl Ether Blends Using Response Surface Methodology," *Energy Fuels*, vol. 31, no. 10, pp. 11362–11376, Oct. 2017, doi: 10.1021/acs.energyfuels.7b01515.

[6] N. Bhanu Teja and N. Alagumurthi, "Emission, performance and combustion study on watermelon methyl ester in diesel engine," *Int. J. Ambient Energy*, vol. 42, no. 3, pp. 285–291, Feb. 2021, doi: 10.1080/01430750.2018.1542628.

[7] A.K. Srivastava, S.L. Soni, D. Sharma, and N.L. Jain, "Effect of injection pressure on performance, emission, and combustion characteristics of diesel–acetylene-fuelled single cylinder

stationary CI engine," *Environ. Sci. Pollut. Res.*, vol. 25, no. 8, pp. 7767–7775, Mar. 2018, doi: 10.1007/s11356-017-1070-3.

[8] J.Y. Kim, G. Park, S. Jung, Y.F. Tsang, and E.E. Kwon, "Direct conversion process for enhancing biodiesel production from insect biomass waste," *Appl. Energy*, vol. 380, p. 125136, Feb. 2025, doi: 10.1016/j.apenergy.2024.125136.

[9] G. Dhamodaran and A. Elumalai, "Effect of ternary nanocomposite in margosa biodiesel microemulsion blends on performance, emission, and combustion characteristics of a diesel engine," *Energy*, vol. 326, p. 136362, Jul. 2025, doi: 10.1016/j.energy.2025.136362.

[10] K. Muralidharan and D. Vasudevan, "Performance, emission and combustion characteristics of a variable compression ratio engine using methyl esters of waste cooking oil and diesel blends," *Appl. Energy*, vol. 88, no. 11, pp. 3959–3968, Nov. 2011, doi: 10.1016/j.apenergy.2011.04.014.

[11] C.D. Rakopoulos, K.A. Antonopoulos, D.C. Rakopoulos, D.T. Hountalas, and E.G. Giakoumis, "Comparative performance and emissions study of a direct injection Diesel engine using blends of Diesel fuel with vegetable oils or bio-diesels of various origins," *Energy Convers. Manag.*, vol. 47, no. 18–19, pp. 3272–3287, Nov. 2006, doi: 10.1016/j.enconman.2006.01.006.

[12] R.R. Renish, A.J. Selvam, R. Čep, and M. Elangovan, "Influence of Varying Compression Ratio of a Compression Ignition Engine Fueled with B20 Blends of Sea Mango Biodiesel," *Processes*, vol. 10, no. 7, p. 1423, Jul. 2022, doi: 10.3390/pr10071423.

[13] S. Şimsek, G. Gürüf, S. Uslu, and H. Şimsek, "Exergy, exergoeconomic, enviroeconomic, and sustainability index analysis of diesel engine fueled by binary combinations of diesel/waste animal fat biodiesel," *J. Therm. Anal. Calorim.*, vol. 148, no. 15, pp. 7767–7780, Aug. 2023, doi: 10.1007/s10973-023-12273-3.

[14] J.G. Alotaibi, A.E. Alajmi, T. Alsaeed, S.H. Al-Lwayzy, and B.F. Yousif, "On the Influence of Engine Compression Ratio on Diesel Engine Performance and Emission Fueled with Biodiesel Extracted from Waste Cooking Oil," *Energies*, vol. 17, no. 15, p. 3844, Aug. 2024, doi: 10.3390/en17153844.

[15] C.S. Lee, S.W. Park, and S. Il Kwon, "An Experimental Study on the Atomization and Combustion Characteristics of Biodiesel-Blended Fuels," *Energy Fuels*, vol. 19, no. 5, pp. 2201–2208, Sep. 2005, doi: 10.1021/ef050026h.

[16] H. Kurji *et al.*, "Combustion characteristics of biodiesel saturated with pyrolysis oil for power generation in gas turbines," *Renew. Energy*, vol. 99, pp. 443–451, Dec. 2016, doi: 10.1016/j.renene.2016.07.036.

[17] N.A. Fathurrahman *et al.*, "Lubricity Properties of Palm Oil Biodiesel Blends with Petroleum Diesel and Hydrogenated Vegetable Oil," *Lubricants*, vol. 11, no. 4, p. 176, Apr. 2023, doi: 10.3390/lubricants11040176.

[18] A.S. El-Shafay, Ü. Ağbulut, E.-A. Attia, K.L. Touileb, and M.S. Gad, "Waste to energy: Production of poultry-based fat biodiesel and experimental assessment of its usability on engine behaviors," *Energy*, vol. 262, p. 125457, Jan. 2023, doi: 10.1016/j.energy.2022.125457.

[19] J.B. Heywood, *Internal Combustion Engine Fundamentals*, 2nd ed. New York: McGraw-Hill, 2018.

[20] T.K. Sahu, S. Sarkar, and P.C. Shukla, "Combustion investigation of waste cooking oil (WCO) with varying compression ratio in a single cylinder CI engine," *Fuel*, vol. 283, p. 119262, Jan. 2021, doi: 10.1016/j.fuel.2020.119262.

[21] N.S. Dugala, G.S. Goindi, and A. Sharma, "Experimental investigations on the performance and emissions characteristics of dual biodiesel blends on a varying compression ratio diesel engine," *SN Appl. Sci.*, vol. 3, no. 6, p. 622, Jun. 2021, doi: 10.1007/s42452-021-04618-0.

[22] B. Doğan, S.G. Ghanati, M.K. Yeşilyurt, and H. Yaman, "Effects of compression ratio on the performance and emission levels of a CI engine fueled with safflower oil methyl ester through an engine simulation approach," *Sci. Technol. Energy Transit.*, vol. 79, p. 16, Mar. 2024, doi: 10.2516/stet/2024015.

[23] J.G. Alotaibi, A.E. Alajmi, T. Alsaeed, S.H. Al-Lwayzy, and B.F. Yousif, "On the Influence of Engine Compression Ratio on Diesel Engine Performance and Emission Fueled with Biodiesel Extracted from Waste Cooking Oil," *Energies*, vol. 17, no. 15, p. 3844, Aug. 2024, doi: 10.3390/en17153844.

[24] G. Prasada Rao and L. Sathya Vara Prasad, "Combined influence of compression ratio and exhaust gas recirculation on the diverse characteristics of the diesel engine fueled with novel palmyra biodiesel blend," *Energy Convers. Manag.: X*, vol. 14, p. 100185, May 2022, doi: 10.1016/j.ecmx.2022.100185.

[25] S. Ashfaque Ahmed *et al.*, "Investigation of ternary blends of animal fat biodiesel-diethyl ether-diesel fuel on CMFIS-CI engine characteristics," *Fuel*, vol. 332, p. 126200, Jan. 2023, doi: 10.1016/j.fuel.2022.126200.

[26] K. Masera and A.K. Hossain, "Advancement of biodiesel fuel quality and NOx emission control techniques," *Renew. Sustain. Energy Rev.*, vol. 178, p. 113235, May 2023, doi: 10.1016/j.rser.2023.113235.

[27] R. Jambulingam, V. Shankar, S. Palani, and G.R. Srinivasan, "Effect of Dominant Fatty Acid Esters on Emission Characteristics of Waste Animal Fat Biodiesel in CI Engine," *Front. Energy Res.*, vol. 7, Jul. 2019, doi: 10.3389/fenrg.2019.00063.